AD_____

Award Number: W81XWH-06-1-0665

TITLE: VEGF-Iron Oxide Conjugate for Dual MR and PET Imaging of Breast Cancer Angiogenesis

PRINCIPAL INVESTIGATOR: Xiaoyuan Chen, Ph.D.

CONTRACTING ORGANIZATION: Stanford University School of Medicine
Stanford, CA 94305

REPORT DATE: September 2007

TYPE OF REPORT: Final

PREPARED FOR: U.S. Army Medical Research and Materiel Command
Fort Detrick, Maryland 21702-5012

REPORT DOCUMENTATION PAGE

Form Approved
OMB No. 0704-0188

1. REPORT DATE *(DD-MM-YYYY)*	**2. REPORT TYPE**	**3. DATES COVERED** *(From - To)*
01-09-2007	Final	1 SEP 2006 - 31 AUG 2007

4. TITLE AND SUBTITLE

VEGF-Iron Oxide Conjugate for Dual MR and PET Imaging of Breast Cancer Angiogenesis

5a. CONTRACT NUMBER

5b. GRANT NUMBER
W81XWH-06-1-0665

5c. PROGRAM ELEMENT NUMBER

6. AUTHOR(S)
Xiaoyuan Chen, Ph.D.

E-Mail: shawchen@stanford.edu

5d. PROJECT NUMBER

5e. TASK NUMBER

5f. WORK UNIT NUMBER

7. PERFORMING ORGANIZATION NAME(S) AND ADDRESS(ES)

Stanford University School of Medicine
Stanford, CA 94305

8. PERFORMING ORGANIZATION REPORT NUMBER

9. SPONSORING / MONITORING AGENCY NAME(S) AND ADDRESS(ES)
U.S. Army Medical Research and Materiel Command
Fort Detrick, Maryland 21702-5012

10. SPONSOR/MONITOR'S ACRONYM(S)

11. SPONSOR/MONITOR'S REPORT NUMBER(S)

12. DISTRIBUTION / AVAILABILITY STATEMENT
Approved for Public Release; Distribution Unlimited

13. SUPPLEMENTARY NOTES

14. ABSTRACT
The overall hypothesis of this concept award proposal is that a single probe that allows simultaneous acquisition of both positron emission tomography (PET) and molecular magnetic resonance imaging (mMRI) data will maximizes the topographical, anatomical, functional, and molecular information of breast cancer. In this proposal, we choose to image breast cancer tumor vasculature by visualization and quantification of Flt-1 and Flk-1/KDR. Objectives: Aim 1: To develop iron oxide (IO) nanoparticles functionalized with both VEGF121 and PET isotope 64Cu (t1/2 = 12.7 h) and test the dual probe in vitro. Aim 2: To test the PET and mMRI efficacy of the dual-functional nanoprobe in breast cancer in vivo. Major Findings: We have developed VEGF121 mutant that is VEGFR-2 specific. We have developed water soluble iron oxide nanoparticles conjugated with macrocyclic chelating agent DOTA for 64Cu-labeling and cyclic RGD peptide for integrin alpha(v)beta(3) recognition. We have also developed IO-VEGF conjugate and tested the nanoconstruct.

15. SUBJECT TERMS
No subject terms provided.

16. SECURITY CLASSIFICATION OF:			**17. LIMITATION OF ABSTRACT**	**18. NUMBER OF PAGES**	**19a. NAME OF RESPONSIBLE PERSON**
a. REPORT	**b. ABSTRACT**	**c. THIS PAGE**			USAMRMC
U	U	U	UU	18	**19b. TELEPHONE NUMBER** *(include area code)*

Table of Contents

INTRODUCTION

Breast cancer is the most common form of cancer in women. Despite vigorous efforts to diagnose, treat and prevent this disease, it remains a leading cause of death among women. Vascular endothelial growth factor (VEGF) and its receptors are essential for breast cancer angiogenesis and metastasis. The angiogenic actions of VEGF are mediated via two closely related endothelium-specific receptor tyrosine kinases, Flk-1/KDR and Flt-1. Both are largely restricted to vascular endothelial cells. It has been reported that both Flk-1/KDR and Flt-1 receptors are overexpressed on the endothelium of breast cancer vasculature, whereas they are almost undetectable in the vascular endothelium of adjacent normal tissues. The ability to non-invasively visualize and quantify tumor VEGF receptor expression level will provide new opportunities to document breast cancer angiogenesis status, more appropriately select patients considered for anti-angiogenesis treatment, and monitor anti-angiogenic treatment efficacy. We have recently demonstrated that recombinant human $VEGF_{121}$ can be labeled with positron emitting radionuclide ^{64}Cu without loss of receptor affinity and functional activity of the protein. ^{64}Cu-VEGF is also able to delineate small tumors that are highly angiogenic. Although highly sensitive, positron emission tomography (PET) has relatively poor spatial resolution. Magnetic resonance imaging (MRI), on the other hand, provides exquisite high-resolution anatomical information, as well as access to volume specific chemical and physical information. Functional MRI is thus an excellent tool for assessing tumor angiogenesis and blood flow. Furthermore, signal amplification techniques have enabled both T_2 and T_1 mediated molecular MRI (mMRI), thus extending MRI further beyond the anatomical and physiological level.

We **hypothesize** that a single probe that allows simultaneous acquisition of both PET and mMRI data will maximizes the topographical, anatomical, functional, and molecular information of breast cancer. In this proposal, we choose to image breast cancer tumor vasculature by visualization and quantification of Flt-1 and Flk-1/KDR.

Objectives: Aim 1: To develop iron oxide (IO) nanoparticles functionalized with both $VEGF_{121}$ and PET isotope ^{64}Cu ($t_{1/2}$ = 12.7 h) and test the dual probe in vitro. Aim 2: To test the PET and mMRI efficacy of the dual-functional nanoprobe in breast cancer in vivo.

This final report will summarize the major achievements based on the originally proposed studies and further discoveries that derived from this DOD BCRP Concept funding mechanism.

BODY

Part I: Development of VEGFR-2 Specific Mutant

We recently labeled wild-type $VEGF_{121}$, the shortest VEGF-A isoform that exists in nature, with ^{64}Cu ($t_{1/2}$ = 12.7 h) for PET imaging of VEGFR expression (*1*). MicroPET imaging revealed rapid, specific, and prominent uptake of ^{64}Cu-DOTA-$VEGF_{121}$ (~ 15 %ID/g) in highly vascularized small U87MG tumors with high VEGFR-2 expression, but significantly lower and sporadic uptake (~ 3%ID/g) in large U87MG tumors with low VEGFR-2 expression. For this tracer, the highest uptake was in the kidneys. Because the wild-type $VEGF_{121}$ binds to both VEGFR-1 and VEGFR-2 (*2*). The kidney is usually the dose-limiting organ because it has high VEGFR-1 expression, which can take up VEGF-A based tracers (*1, 3, 4*). In our previous study, we found that the uptake of ^{64}Cu-DOTA-$VEGF_{121}$ in the kidneys was mainly due to VEGFR-1 binding (and some renal clearance), while the tumor uptake was mainly related to VEGFR-2 expression (*1*). The high renal uptake may limit its future clinical applications.

Based on alanine scanning mutagenesis, we identified a D63AE64AE67A mutant of $VEGF_{121}$ ($VEGF_{DEE}$) (**Fig. 1**), which binds specifically to VEGFR-2. Cell binding assay reveals that the IC_{50} values of $VEGF_{121}$ and $VEGF_{DEE}$ for VEGFR-1 were 4.2 nM and 78.1 nM, respectively, the IC_{50} values of $VEGF_{121}$ and $VEGF_{DEE}$ for VEGFR-2 were 2.9 nM and 11.7 nM, respectively. Taken together, $VEGF_{DEE}$ has about 20 fold lower VEGFR-1 binding and only 4-fold lower VEGFR-2 binding affinity when compared to $VEGF_{121}$. $VEGF_{121}$ and $VEGF_{DEE}$ were then conjugated with macrocyclic chelating agent 1,4,7,10-tetra-azacylododecane N,N′,N′′,N′′′-tetraacetic acid (DOTA) and labeled with positron emitting radionuclide ^{64}Cu ($t_{1/2}$ = 12.7 h) for positron emission tomography (PET) imaging in an orthotopic 4T1 murine breast cancer model. Quantitative microPET imaging studies indicated that both ^{64}Cu-DOTA-$VEGF_{121}$ and ^{64}Cu-DOTA-$VEGF_{DEE}$ had rapid and prominent activity accumulation in VEGFR-2 expressing 4T1 tumors. The renal uptake of ^{64}Cu-DOTA-$VEGF_{DEE}$ was significantly lower than

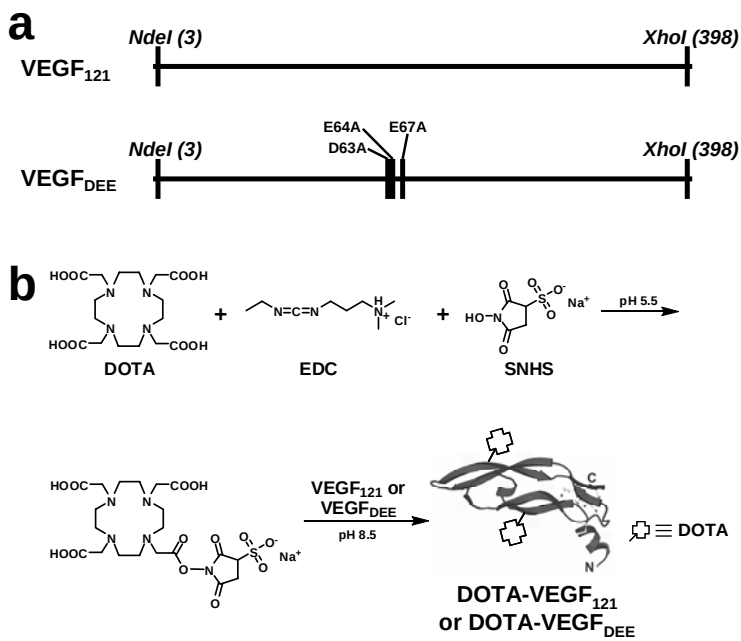

Fig. 1 a Schematic representation of $VEGF_{121}$ and its mutant $VEGF_{DEE}$ (mutated at the 63, 64, and 67 positions). **b** The synthetic scheme of DOTA-$VEGF_{121}$ and DOTA-$VEGF_{DEE}$.

that of ^{64}Cu-DOTA-VEGF$_{121}$ as rodent kidneys expressed high levels of VEGFR-1 based on immunofluorescence staining. Blocking experiments and biodistribution studies confirmed the VEGFR specificity of ^{64}Cu-DOTA-VEGF$_{DEE}$ (**Fig. 2**).

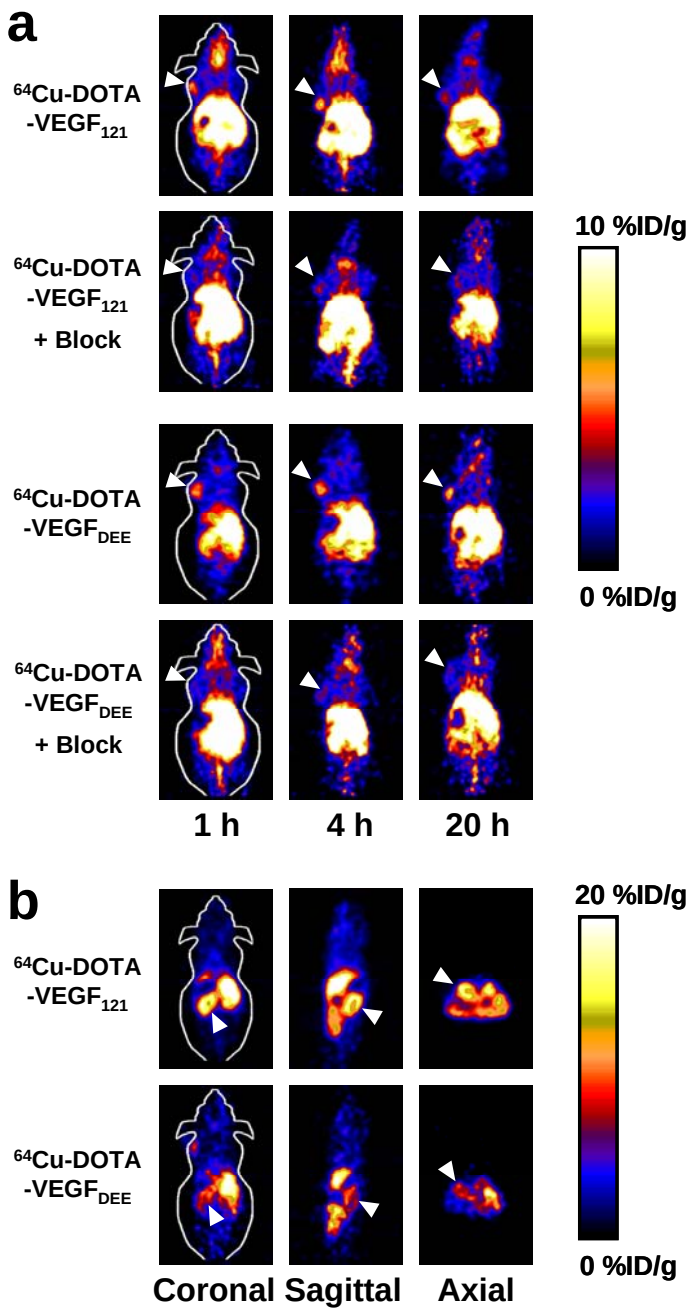

Fig. 2 MicroPET imaging studies of 4T1 tumour-bearing mice. **a** Serial microPET scans of 4T1 tumour-bearing mice injected intravenously with 5-8 MBq of ^{64}Cu-DOTA-VEGF$_{121}$ or ^{64}Cu-DOTA-VEGF$_{DEE}$. Mice co-injected with 200 μg of VEGF$_{121}$ are also shown (denoted as "+ Block"). Coronal slices containing the tumours (arrowheads) are shown. **b** Coronal, sagittal and axial slices containing the kidney (arrowheads) at 4 h post-injection of ^{64}Cu-DOTA-VEGF$_{121}$ or ^{64}Cu-DOTA-VEGF$_{DEE}$. Note the different scale in **a** and **b**.

Part II: Development of Iron Oxide Nanoparticles

We have developed two types of novel superparamagentic iron oxide nanoparticles (USPIO), namely, PVP-IO and PASP-IO.

Polyvinylpyrrolidone (PVP)-coated iron oxide (PVP-IO) nanoparticles were synthesized by a one-step thermal decomposition method (**Fig. 3**). The overall size of the particles is dependent on the PVP/$Fe(CO)_5$ reaction ratio and the core size of the nanoparticles is dependent on the reaction time. In order to prepare stable PVP-IO nanoparticles with large core size and thin coating for macrophage uptake, we found the optimal molar ratio of PVP/$Fe(CO)_5$ to be 0.16 and the reaction time to be 5 h. Moreover large amount of uniform PVP-IO nanoparticles were obtained after acetone purification and dialysis. Transmission electron microscope (TEM) image shows monodisperse PVP-IO with core size of 8-10 nm. Dynamic light scattering (DLS) measurement indicates that the colloidal particles in aqueous solution have hydrodynamic diameter of about 40-50 nm. X-ray diffractometer (XRD) pattern is well indexed to the crystal plane of spinel ferrite. The magnetization curve finds the saturation magnetization of PVP-coated iron oxide nanoparticles to be around 110 emu/g Fe, which is much higher than that of Feridex (ca. 70 emu/g Fe).

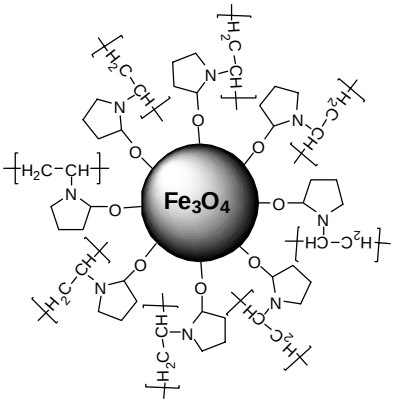

Fig. 3. Schematic structure of PVP-IO.

Transverse T_2 weighted spin echo images were acquired using a 3 Tesla Siemens Tim Trio MR Scanner. A gradient echo acquisition was used with repetition time of 2000 ms, echo time of 1.8 ms, slice thickness of 12 mm, and a flip angle of 20 degrees. The normal first order shim process was applied, and the phantoms were imaged at room temperature. The measured r_2 and r_2* were 174.8 $mM^{-1}s^{-1}$ and 294.3 $mM^{-1}s^{-1}$. It is remarkable that PVP-IO show the highest r_2 among those reported in literature (e.g., r_2 = 151.9 $mM^{-1}s^{-1}$, r_2* = 275.0 $mM^{-1}s^{-1}$ for Feridex). The higher relaxivity of PVP coated

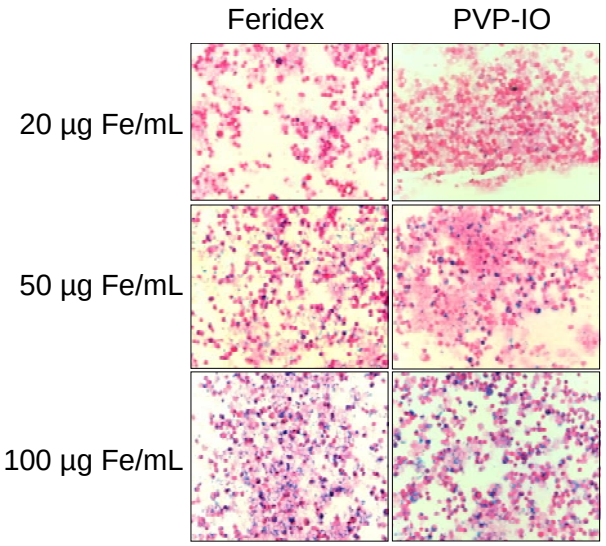

Fig. 4. Mouse macrophage cells were incubated with Feridex or PVP-IO for 48 h at different iron concentrations and then stained by Prussian blue and then counterstained with nuclear fast red. Higher macrophage uptake of large core PVP-IO than Feridex is observed at all concentrations examined.

magnetic nanoparticle is likely attributed to the high magnetic moment of PVP-IO (110 emu/g Fe) and effective magnetic relaxations to the proton spins around PVP-IO.

It is highly desirable that PVP-IO nanoparticles possess high and persistent uptake by macrophages for detection of inflammatory disease by MRI. To investigate this property, in vitro cell uptake experiments were carried out using a mouse macrophage cell line RAW 264.7 (American Type Culture Collection, Manassas, VA). The uptake of PVP-IO by macrophages was compared to that of Feridex that is currently used clinically for MRI. To detect the presence of iron oxide nanoparticles in cells, Prussian blue staining was carried out after 48 h and 72 h of incubation of Feridex and large core PVP-IO nanoparticles with macrophages at 20, 50, and 100 μg/mL. As shown in **Fig. 4**, macrophage uptake of large core PVP-IO is higher than Feridex at all the concentrations examined even though the overall size of PVP-IO is smaller than Feridex.

To confirm the ability of macrophage to take up the newly synthesized large core PVP-IO, the cells were incubated with different concentrations of PVP-IO or Feridex and T_2*-weighted MR images were obtained. As shown in **Fig. 5**, PVP-IO exhibit significantly more negative contrast enhancement as compared to Feridex at relatively low concentrations of Fe. Such difference is diminished when large excess of Fe is used (e.g. 100 mg Fe/mL).

After successful demonstration of the

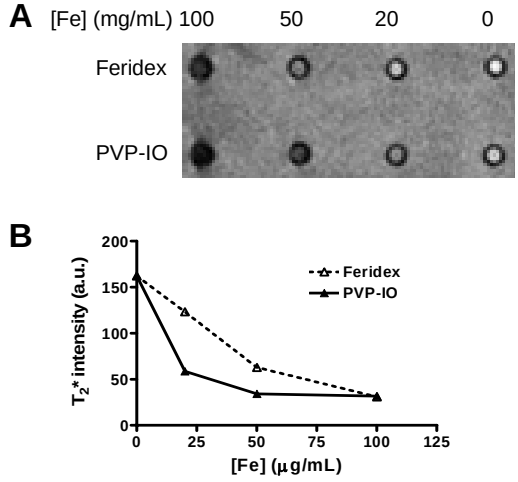

Fig. 5. (A) T_2*-weighted MR images and (B) T_2* MR signal intensity of gelatine gels containing macrophages (1×10^6 cells/well) incubated with Feridex and PVP-coated iron oxide nanoparticles at the different iron concentration. PVP-IO exhibited more negative contrast enhancement as compared to Feridex at relatively low concentrations of Fe.

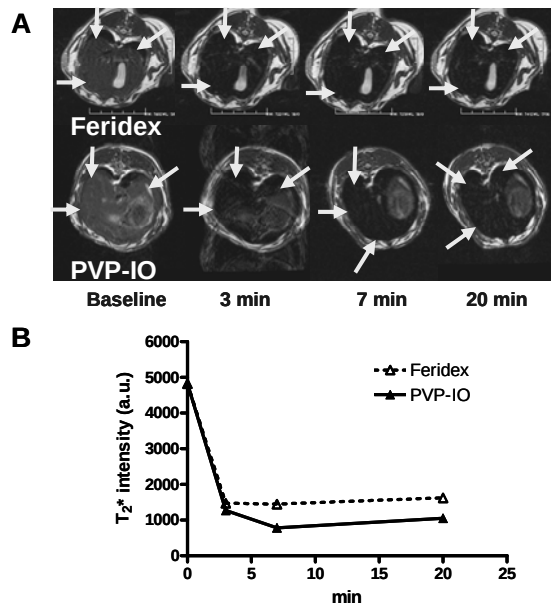

Fig. 6. T2*-weighted MR images before, 3, 7, and 20 min after intravenous injection of Feridex (up) and PVP-coated iron oxide nanoparticles (down).

uptake of large core PVP-IO by macrophages in culture, we tested the same particles in vivo for liver imaging. T_2*-weighted MR images were obtained before and after the administration of large core PVP-IO or Feridex (6 mg Fe/kg) through the marginal vein of rabbits at 3, 7 and 20 min, respectively. Both Feridex and large core PVP-IO are able to lower signal intensity in the rabbit liver parenchyma but the T_2* effect of PVP-IO is more obvious than Feridex (**Fig. 6**).

Poly(aspartic acid) (PASP)-coated IO nanoparticles (PASP-IO) were synthesized using a co-precipitation method and functionalized as shown in **Fig. 7**. TEM revealed that the average size of iron oxide nanoparticles was ~5 nm. A selected area diffraction pattern showed that the iron oxide nanoparticles were Magnetite (Fe_3O_4). In solution, the colloidal particles had a diameter of ~40 nm as determined from DLS data. This data showed that the colloidal particles consisted of iron oxide crystals covered with PASP layer. The hysteresis loop of PASP-coated iron oxide had no coercive force showing superparamagnetic behavior and the saturation magnetization of PASP-coated iron oxide nanoparticles was 116.9 emu/g Fe.

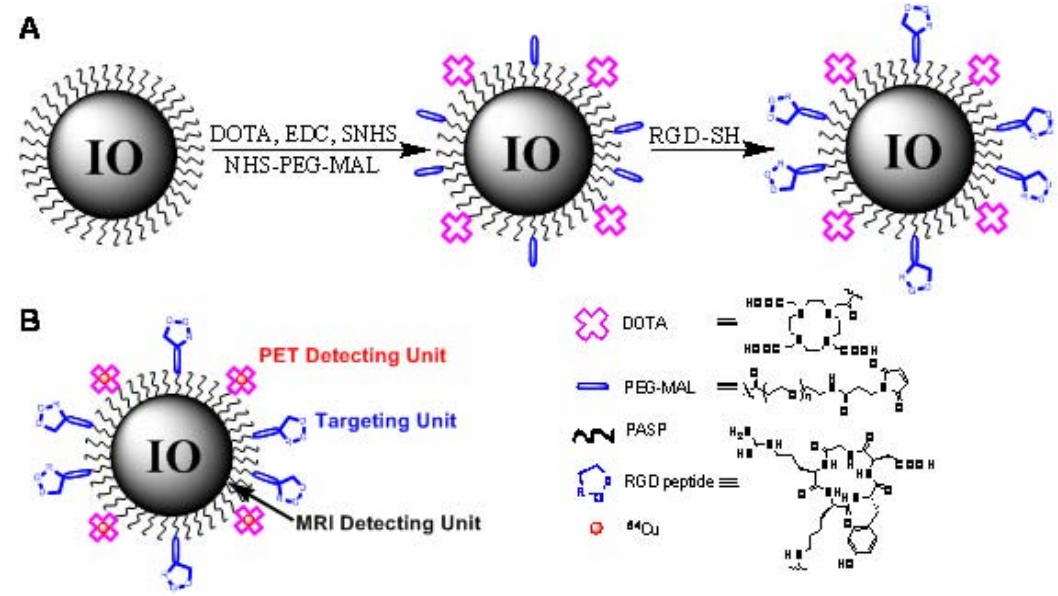

Fig. 7. (A) The synthesis of the PET/MRI dual functional probe DOTA-IO-RGD. DOTA-IO was prepared similarly except that no RGD peptide was used. (B) Illustration of PET/MRI probe based on iron oxide nanoparticle.

The signal contrast enhancement effect of T_2- and T_1-weighted MR images of PASP-IO and Feridex in a same concentration gradient in distilled water ranging from 4×10^{-4} to 1.25×10^{-5} M iron concentration is shown in **Fig. 8**. T_2 signal intensity of PASP-IO was reduced faster than Feridex at the lower iron concentration and T_1 signal intensity was increased faster than Feridex at the lower concentration, showing that PASP-IO could be used as both a T_2 and T_1 contrast agent. Transverse T_2 weighted spin echo images were acquired using a 3 Tesla Siemens Tim Trio MR Scanner. The measured r_2 and r_2* were $105.5 mM^{-1}s^{-1}$ and $165.5 mM^{-1}s^{-1}$, respectively, which were somewhat lower than Feridex (r_2 = 151.9 $mM^{-1}s^{-1}$, r_2* = 275.0 $mM^{-1}s^{-1}$).

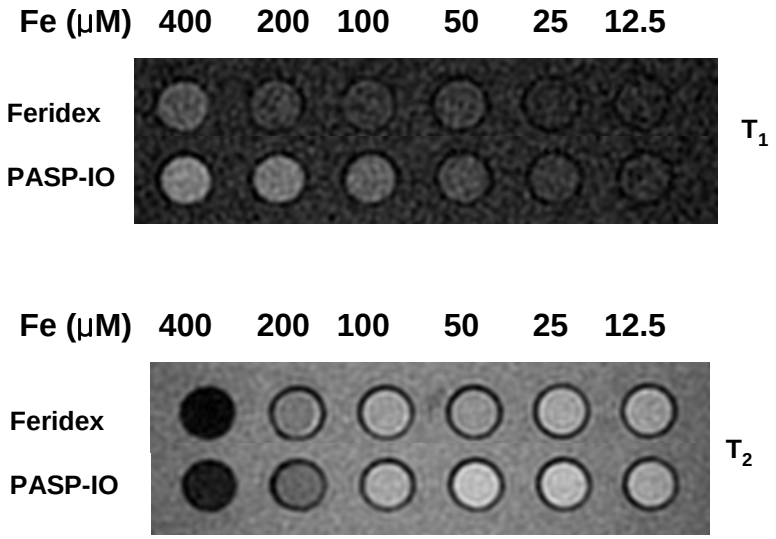

Fig. 8. Phantom image acquired from T_1 weighted MR scan (up) and T_2 weighted MR scan (down) for Feridex and PASP-IO at the different iron concentrations.

Part III: Development of IO conjugates for tumor angiogenesis imaging

Polyaspartic acid (PASP) has two kinds of functional groups: carboxylates (-COOH) and amines ($-NH_2$). Therefore, iron oxide nanoparticles were coated with PASAP through the carboxyl group and the remaining amine group were used for DOTA or hetero-linker conjugation with NHS-PEG-MAL. The maleimide residues on the IO surface were then coupled with RGD-SH through Michael addition reaction. The DOTA-IO-RGD conjugate showed integrin specificity according to cell based receptor binding assay (**Fig. 9**).

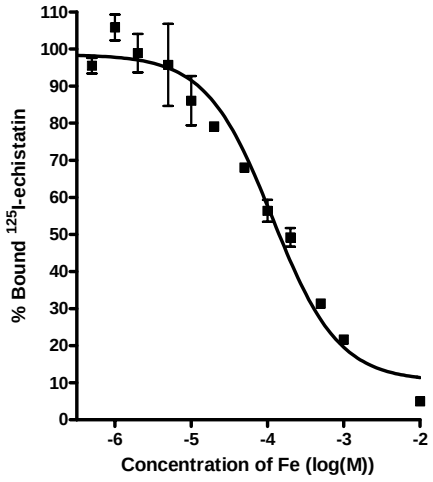

Fig. 9. Inhibition of ^{125}I-echistatin (integrin $\alpha_v\beta_3$ specific) binding to integrin $\alpha_v\beta_3$ on U87MG cells by DOTA-IO-RGD (n = 3, mean ± SD).

Fig. 10 shows coronal microPET images of a female mouse at different time points after injection of 3.7 mBq radiotracer. All microPET images were decay corrected and the tumor was clearly visualized with high contrast relative to the contralateral background from 1 to 21 h after injection of ^{64}Cu-DOTA-IO-RGD in U87MG tumor mice. Compared with the RGD conjugated nanoparticle, the non-targeted particle ^{64}Cu-DOTA-IO showed significantly lower tumor uptake which might be caused by passive targeting. Tumor accumulation 1 h after injection of ^{64}Cu-DOTA-IO-RGD was 7.9 $\pm$ 0.8 percentage injected dose per gram (%ID/g) and steadily increased and peaked at

about 4 h after injection (10.1 ± 2.1 %ID/g). At 21 h after injection, tumor uptake slightly decreased to 9.8 ± 3.2 %ID/g. A blocking experiment with 200 μg of RGD injected before ^{64}Cu-DOTA-IO-RGD revealed a significant reduction in ^{64}Cu-DOTA-IO-RGD uptake.

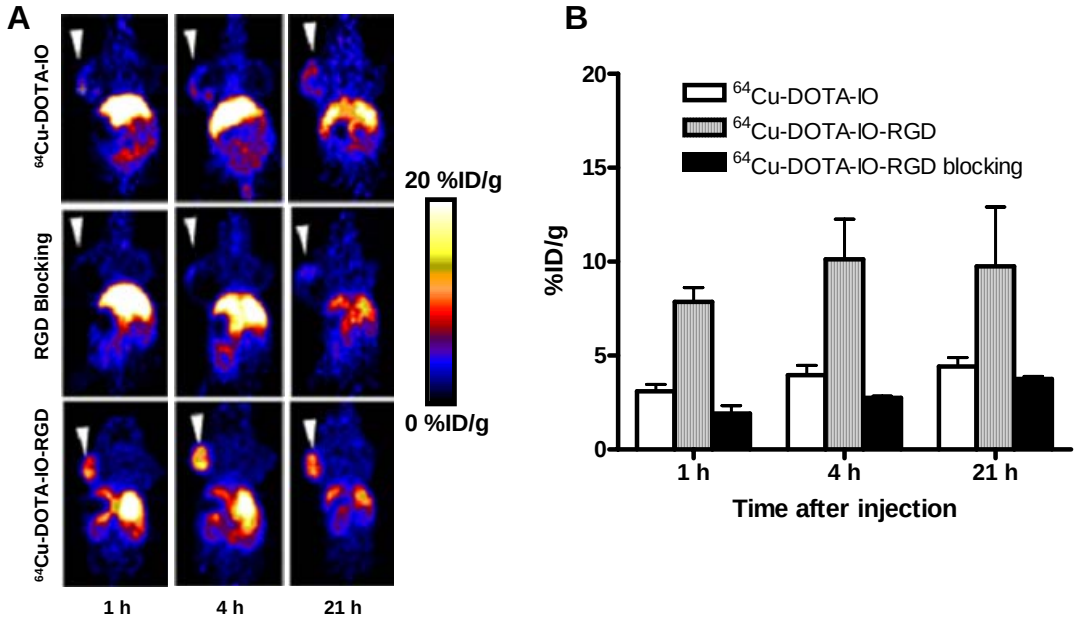

Fig. 10. (A) Decay-corrected whole-body coronal microPET images of nude mouse bearing human U87MG tumor at 1, 4, and 21 h after injection of 3.7 MBq of ^{64}Cu-DOTA-IO, ^{64}Cu-DOTA-IO-RGD or ^{64}Cu-DOTA-IO-RGD with blocking dose of cold c(RGDyK) peptide. (B) Time-activity curves of U87MG tumor after injection of 3.7 MBq of ^{64}Cu-DOTA-IO, ^{64}Cu-DOTA-IO-RGD or ^{64}Cu-DOTA-IO-RGD with blocking dose of cold c(RGDyK) peptide.

To investigate the integrin $\alpha_v\beta_3$ targeting ability and MRI visibility of DOTA-IO-RGD conjugates, *in vivo* T2-weighted fast spin-echo MR imaging was performed with mice bearing U87MG tumors (**Fig. 11**). MR signal intensity decreased significantly after injection of DOTA-IO-RGD as compared with IO injection and DOTA-IO-RGD co-administration with integrin $\alpha_v\beta_3$ blocking agent. Signal intensity decreased after injection with IO and had a different distribution pattern compared with DOTA-IO-RGD with particle accumulation predominantly at the lateral tumor borders. MR signal intensity also decreased slightly after injection of free ligand to block integrin $\alpha_v\beta_3$ receptors followed by administration of DOTA-IO-RGD.

Uptake of PASP-IO, DOTA-IO-RGD, and DOTA-IO-RGD plus free RGD was assessed histologically using Prussian blue staining (**Fig. 12**). After 20 min, blue spots on the surface of U87MG cells were observed, indicating a strong uptake of DOTA-IO-RGD, whereas there was no significant uptake for plain particles. Blocking integrin $\alpha_v\beta_3$ receptors with free RGD effectively reduced the number of blue spots on the surface of U87MG cells, showing that the accumulation of PASP-IO-RGD was specifically mediated by its integrin $\alpha_v\beta_3$ binding. Prussian Blue staining was also performed with different tissue slides such as tumor, liver, spleen, muscle, and kidney after injection of

DOTA-IO-RGD or DOTA-IO. In the liver and spleen, both DOTA-IO-RGD and DOTA-IO had significant uptake with no visible difference between the two particles.

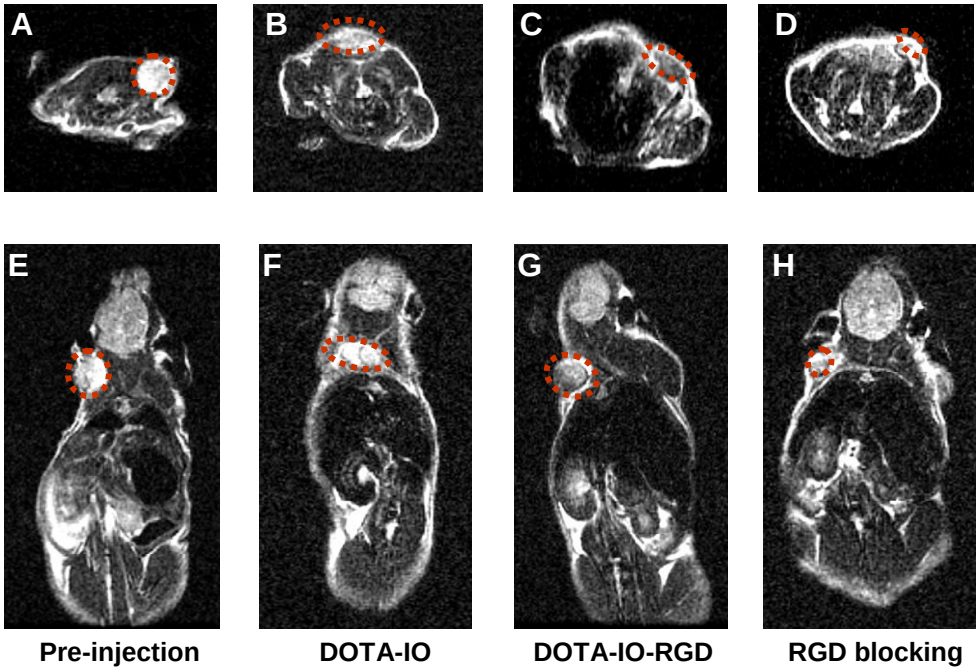

Fig. 11. T_2-weighted MR images of nude mice bearing U87MG tumor before injection of iron oxide nanoparticle(A, E) and 4 h after tail vain injection of DOTA-IO (B, F), DOTA-IO-RGD (C, G), and DOTA-IO-RGD with blocking dose of cold c(RGDyK) peptide (D, H).

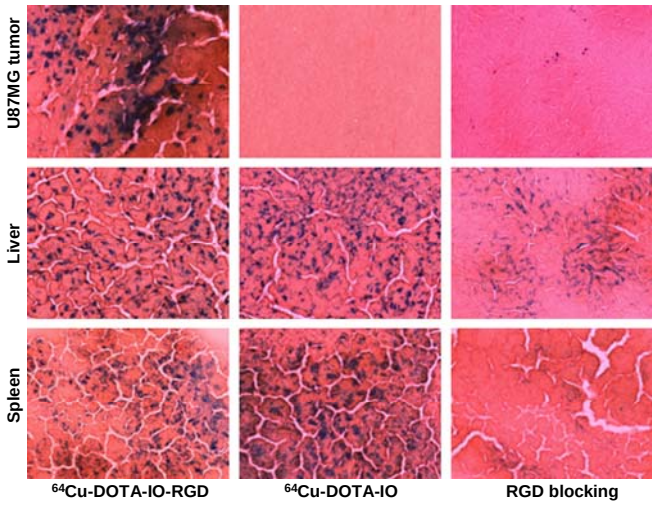

Fig. 12. Prussian blue stained U87MG tumor, liver and spleen after injection of ^{64}Cu-DOTA-IO-RGD, ^{64}Cu-DOTA-IO, and ^{64}Cu-DOTA-IO-RGD with blocking dose of cold c(RGDyK) peptide.

We have also developed DOTA-IO-$VEGF_{121}$ conjugate. To evaluate the binding affinity of DOTA-IO-$VEGF_{121}$ for VEGFR, Prussian blue staining on the porcine aorta endothelial (PAE) cells (VEGFR negative) and PAE/KDR cells (PAE cells stably transfected with VEGFR-2) were carried out in 6-well Chamber slides, respectively.

PAE or PAE/KDR cells were incubated with DOTA-IO-VEGF$_{121}$ or DOTA-IO for 30 min at the 30 μM Fe concentration and cells were then washed 3 times with PBS and dried at 37 °C for 4 h. The attached cells were then incubated with 10% potassium ferrocyanide in 20% hydrochloric acid for 20 min and washed in distilled water 3 times. The cells were incubated with 1 % eosin solution for 10 min and washed in distilled water for counterstaining with nuclear fast red. For dehydration, the cells were incubated with absolute ethanol for 3-5 min. Mounting medium was then placed on the slides along with a coverslip and the iron particles in cells were observed as blue dots using an optical microscope with phase contrast. Only PAE/KDR cells showed prominent staining of DOTA-IO-VEGF, demonstrating VEGFR specificity of this iron oxide conjugate. In vivo test of this conjugate in breast cancer models is currently in progress.

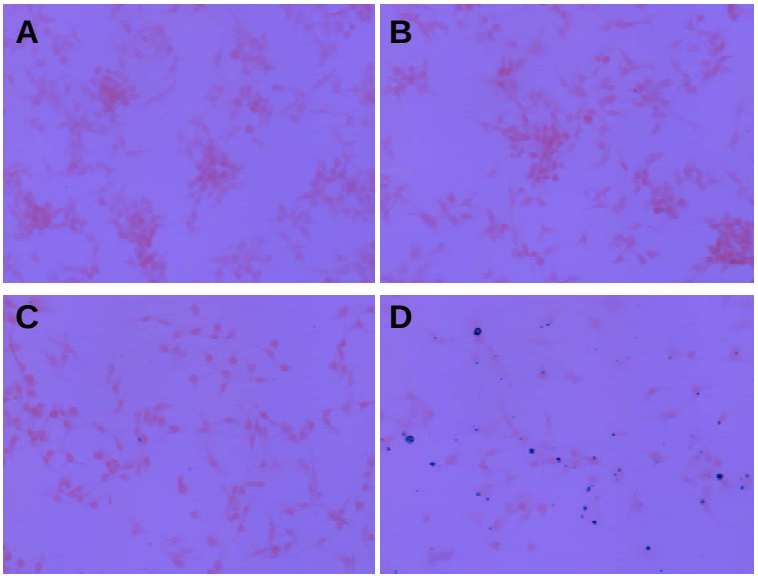

Fig. 13. Prussian blue staining of PAE (A, B) and PAE/KDR (C, D) cells with DOTA-IO (A, C) and DOTA-IO-VEGF$_{121}$ (B, D).

KEY RESEARCH ACCOMPLISHMENTS

- We have successfully produced both wild-type $VEGF_{121}$ protein and VEGFR-2 specific mutant $VEGF_{DEE}$ by recombinant technique.
- We have developed two types of novel iron oxide nanoparticles PVP-IO and PASP-IO;
- Polyvinylpyrrolidone (PVP)-coated iron oxide (PVP-IO) nanoparticles outperforms Feridex for macrophage targeting;
- Poly(aspartic acid) (PASP)-coated iron oxide (PASP-IO) nanoparticles were simultaneously conjugated with tumor vasculature specific ligands $VEGF_{121}$ and cyclic RGD peptide as well as macrocyclic chelating agent DOTA for MR and PET dual modality imaging.

REPORTABLE OUTCOMES

Publications:

1. Wang H, Cai W, Chen K, Li Z-B, He L, **Chen X**. A new PET tracer specific for vascular endothelial growth factor receptor 2. *Eur J Nucl Med Mol Imaging* 2007 Aug 11; [Epub ahead of print].
2. Cai W, **Chen X**. Multimodality imaging of vascular endothelial growth factor and vascular endothelial growth factor receptor expression. *Front Biosci.* 2007;12:4267-4279.
3. Cai W, Chen K, Mohamedali KA, Cao Q, Gambhir SS, Rosenblum MG, **Chen X**. ^{64}Cu-Labeled $VEGF_{121}$ for Positron Emission Tomography Imaging of VEGFR Expression. *J Nucl Med.* 2006;47:2048-2056.
4. Cai W, **Chen X**. Nanoplatforms for Targeted Molecular Imaging in Living Subjects. *Small* 2007 Oct 17; [Epub ahead of print].
5. Lee H-Y, Lee, S-H, Xu C, Xie J, Lee J-H, Wu B, Koh AL, Wang X, Wang SX, Nishimura DG, Biswal S, Sun S, Cho SH, **Chen X**. In Vitro and In Vivo Test of PVP-coated Large Core Iron Oxide Nanoparticles as Macrophage Specific MRI Contrast Agent. *Small* (submitted, 2007).
6. Lee H-Y, Li Z-B, Chen K, Hsu AR, Xu C, Xie J, Sun S, **Chen X**. PET/MRI Dual Modality Tumor Imaging Using Conjugated Radiolabeled Iron Oxide Nanoparticles. *J Nucl Med* (submitted, 2007).

Abstracts:

1. Lee H-Y, Lee SH, Lee J-H, Koh AL, Wu B, Wang X, Wang S, Nishimura DG, Biswal S, Cho SH, Chen X
   In Vitro and In Vivo Test of PVP-coated Iron Oxide Nanoparticles as Liver-Specific MRI Contrast Agent
   Joint Molecular Imaging Conference, Providence, Rhode Island, September 2007
2. Lee H-Y, Li Z-B, Chen K, Lee S-H, Lee J-H, Nishimura DG, Cho SH, Biswal S, Chen X
   Radiolabeled Iron Oxide Nanoparticle Conjugate for PET/MRI Dual Modality Imaging of Tumor Vasculature
   Joint Molecular Imaging Conference, Providence, Rhode Island, September 2007
3. Wang H, Cai W, Chen K, Li Z-B, He L, Chen X
   A VEGFR2 Specific PET Tracer
   Joint Molecular Imaging Conference, Providence, Rhode Island, September 2007

CONCLUSIONS

We have designed, synthesized, and tested a novel bifunctional iron oxide-based nanoprobe for dual PET/MRI imaging of tumor angiogenesis markers integrin $\alpha_v\beta_3$ and VEGFR-2. The success of this imaging approach may allow for early clinical tumor detection with a high degree of sensitivity while also providing anatomic and molecular information specific to the tumor of interest.

REFERENCES

1. Cai W, Chen K, Mohamedali KA, et al. PET of vascular endothelial growth factor receptor expression. *J Nucl Med.* 2006;47(12):2048-2056.

2. Hurwitz H, Fehrenbacher L, Novotny W, et al. Bevacizumab plus irinotecan, fluorouracil, and leucovorin for metastatic colorectal cancer. *N Engl J Med.* Jun 3 2004;350(23):2335-2342.

3. Simon M, Rockl W, Hornig C, et al. Receptors of vascular endothelial growth factor/vascular permeability factor (VEGF/VPF) in fetal and adult human kidney: localization and [^{125}I]VEGF binding sites. *J Am Soc Nephrol.* Jun 1998;9(6):1032-1044.

4. Backer MV, Levashova Z, Patel V, et al. Molecular imaging of VEGF receptors in angiogenic vasculature with single-chain VEGF-based probes. *Nat Med.* Mar 11 2007;13(4):504-509.

APPENDICES

None.